Temperature-Driven Gapless Topological Insulator

Miguel Gonçalves,[1] Pedro Ribeiro,[1,2] Rubem Mondaini,[2] and Eduardo V. Castro[1,2,3]
[1]*CeFEMA, Instituto Superior Técnico, Universidade de Lisboa, Avenida Rovisco Pais, 1049-001 Lisboa, Portugal*
[2]*Beijing Computational Science Research Center, Beijing 100084, China*
[3]*Centro de Física das Universidades do Minho e Porto, Departamento de Física e Astronomia, Faculdade de Ciências, Universidade do Porto, 4169-007 Porto, Portugal*

(Received 6 September 2018; revised manuscript received 11 December 2018; published 28 March 2019)

We investigate the phase diagram of the Haldane-Falicov-Kimball model—a model combining topology, interactions, and spontaneous disorder at finite temperatures. Using an unbiased numerical method, we map out the phase diagram on the interaction-temperature plane. Along with known phases, we unveil an *insulating charge ordered state with gapless excitations* and a temperature-driven *gapless topological insulating* phase. Intrinsic—temperature-generated—disorder is the key ingredient explaining the unexpected behavior. Our findings support the possibility of having temperature-driven topological transitions into gapped and gapless topological insulating phases in mass unbalanced systems with two fermionic species.

DOI: 10.1103/PhysRevLett.122.126601

Understanding the effects of disorder, interactions, and temperature on topological phases of matter is essential to predict the topological properties and their stability in real-world materials [1]. Some of these effects are quite subtle and may have dichotomic features. For example, topological phases are suppressed in the presence of strong nearest-neighbor (NN) [2] or Hubbard-like interactions [3–12]. However, interaction-induced magnetic order was found to coexist with topological phases [13–16], and some studies showed that interactions themselves could induce a topological phase on a trivial band, forming the so-called topological Mott insulator [17–24]. Even if this phase is disputed outside the mean-field scope in some models [25–28], it has been confirmed in others [29,30].

The influence of correlations at finite temperatures on topological insulators (TIs) also shows opposite trends [31–34]. Although thermal fluctuations are responsible for the destruction of topological order when large enough [35,36], they can also drive different types of topological phases [31,37].

The role of disorder on topological phases is also subtle. For TIs within the unitary class [38–40] (for which time-reversal symmetry is broken), disorder effects localize every eigenstate except two bulk extended states that carry opposite Chern numbers [41,42]. The merging of these states, for a sufficiently large disorder strength, is associated with the destruction of the topological phase. Interestingly, a disorder-induced transition into a new topologically nontrivial phase—the topological Anderson insulator (TAI)—was also proposed [43–47].

In this Letter, we explore some of the dichotomic aspects above by fully characterizing an interacting quantum model that crucially combines nontrivial topology, disorder, temperature, and interaction effects and which can be efficiently studied by unbiased numerical methods. Our main results are summarized in Fig. 1, which depicts the different phases as a function of the temperature T and of the interaction magnitude U. As a central result, topological order was found for intermediate U values when T is

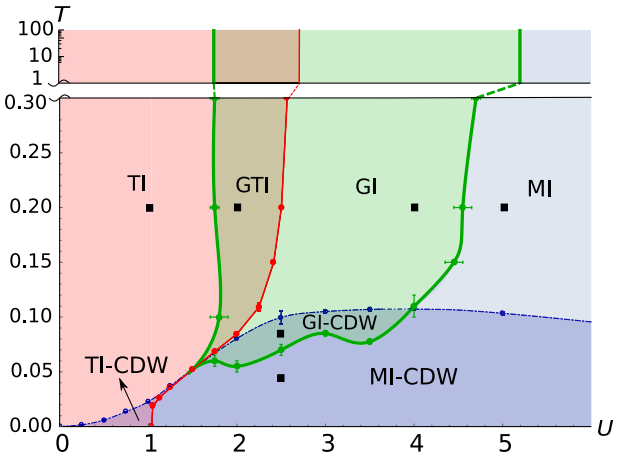

FIG. 1. Phase diagram of the HFKM in the interaction-temperature plane obtained with the Monte Carlo method. Phases at intermediate to high T, outside the CDW: TI for small U, GTI and gapless insulator (GI) for intermediary U, and Mott-like insulating phase (MI) for large U. Phases at low T, inside the CDW phase: Phases with similar features as their high-T counterparts were found, and the suffix "-CDW" was added. The thin (red) and dashed-dotted (blue) curves correspond, respectively, to the topological and CDW phase transitions, and the thick (green) curve bounds the gapless region of the phase diagram. The black squares mark the points used in Figs. 2(b)–2(d).

increased and to extend into the gapless region of the phase diagram at higher T, giving rise to a *temperature-driven gapless topological insulating phase* (GTI).

Model.—Our starting point is the Falicov-Kimball model (FKM) [48], a limiting case of the Hubbard model for which one of the spin fermion species is infinitely massive, rendering these fermions—the f electrons—immobile. For a half-filled bipartite lattice at $T = 0$, the f electrons order in a charge density wave (CDW) state for any finite value of the interaction strength between the localized and itinerant electrons [49–52]. Recently, the full T-dependent phase diagram of the 2D FKM was obtained, unveiling an Anderson insulating phase overlooked in previous studies [53]. The itinerant electrons experience a potential imposed by annealed f-electron configurations, able to localize the c-electron eigenstates in an explicit disorder-free setup. We combine the interacting nature of the FKM with the topological features of the first theoretical model of a TI under a zero net magnetic field—the Haldane model [54]—which, although robust to small disorder, has its topological properties destroyed for large enough disorder strengths [55–58].

The Hamiltonian of the Haldane-Falicov-Kimball model (HFKM) is defined as

$$\hat{H} = -t\sum_{\langle i,j\rangle}\hat{c}_i^\dagger\hat{c}_j + \mathrm{i}t_2\sum_{\langle\langle i,j\rangle\rangle}\nu_{ij}\hat{c}_i^\dagger\hat{c}_j + \mathrm{H.c.} + U\sum_i\hat{c}_i^\dagger\hat{c}_i n_i^f - \sum_i(\mu_c\hat{c}_i^\dagger\hat{c}_i + \mu_f n_i^f), \quad (1)$$

depicting a species of itinerant electrons (c electrons) with creation operators $\hat{c}_i^\dagger$ and another of localized electrons (f electrons) whose local density at site i is n_i^f. The operators $\hat{c}_i^\dagger = \hat{c}_{i,A}^\dagger, \hat{c}_{i,B}^\dagger$ are defined in the two interpenetrating triangular sublattices A and B that form the honeycomb lattice shown in the sketch in Fig. 2(a), with total volume $V = 2L^2$, where L indicates the linear number of unit cells. The first term is the kinetic energy of c electrons associated with NN hoppings, with t being the hopping integral for NN. The second term considers Haldane next-nearest-neighbor (NNN) complex hoppings with $\nu_{ij} = \pm 1$, according to the arrows represented in the honeycomb cell in Fig. 2(a). The third term describes the local interaction between localized and itinerant electrons, with $U > 0$. The final term contains the chemical potentials for the itinerant and localized electrons, respectively, μ_c and μ_f, which we set to $U/2$ (half filling). In what follows, $t = 1$ sets the energy scale and $t_2 = 0.1t$.

Given that the f-electron densities n_i^f $(= 0, 1)$ can be seen as classical variables, the partition function can be written as

$$\mathcal{Z} = \sum_{\{n_f\}}\mathrm{Tr}_c[e^{-\beta\hat{H}(\{n_f\})}] = \sum_{\{n_f\}}e^{-\beta\mathcal{H}(\{n_f\})}, \quad (2)$$

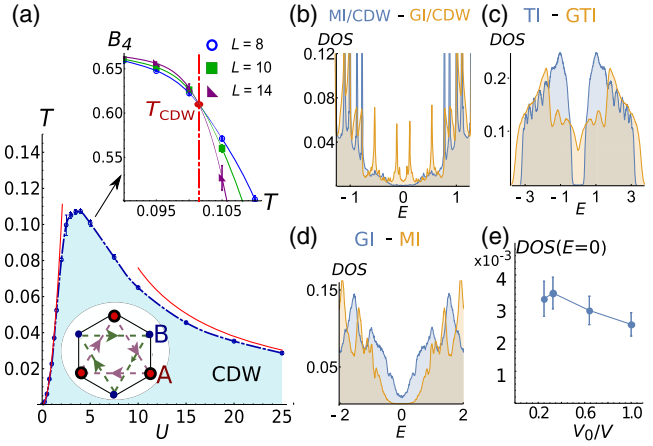

FIG. 2. (a) Monte Carlo results of the CDW phase transition along with the small and large U curves obtained with the second-order perturbation theory [59]. The larger sites in the honeycomb unit cell inside the CDW phase represent occupied sites indicating a checkerboard order; the arrows represent the flow of NNN hoppings. The inset shows an example of the usage of the Binder cumulant method to compute the critical temperature T_{CDW} that corresponds to the intersection of the obtained curves for different system sizes, for a case where $U = 5$. (b)–(d) Density of states for different points in the phase diagram, marked with black squares in Fig. 1: MI-CDW $(U, T) = (2.5, 0.045)$, GI-CDW (2.5,0.085), TI (1,0.2), GTI (2,0.2), GI (4,0.2), and MI (5,0.2); we use a Lorentzian broadening of width 0.01. (e) Finite-size scaling of the DOS at $E = 0$ for the point (2.5,0.085) used in (b). The DOS $(E = 0)$ was computed in an energy window corresponding to 1% of the full bandwidth for $L = 8$ (smallest used system, with volume V_0). This window was reduced proportionally to the system size for larger systems.

where

$$\mathcal{H}(\{n_f\}) = -\frac{U}{2}\sum_i n_i^f - \frac{1}{\beta}\sum_j \ln[1 + e^{-\beta E_j(\{n_f\})}] \quad (3)$$

is the effective Hamiltonian obtained after tracing over the c electrons' degrees of freedom and is defined in terms of the eigenvalues $E_j(\{n_f\})$ of $\hat{H}(\{n_f\})$, corresponding to eigenvectors $|\phi^j(\{n_f\})\rangle$, for a fixed configuration $\{n_f\}$. In this form, the model is amenable to classical Monte Carlo sampling, since, for each configuration $\{n_f\}$, the eigenfunction of the c electrons is given by a simple Slater determinant.

Observables.—For the f electrons, we focus on describing the CDW phase transition, characterized by an order parameter corresponding to $n_{\mathrm{st}}^f = n_A^f - n_B^f$, where n_x^f is the f-electron density in sublattice x. The critical T curve $T_{\mathrm{CDW}}(U)$ is obtained by fixing U and computing the intersections of the T-dependent Binder cumulant, $B_4 = (1 - \langle n_{\mathrm{st}}^{f\,4}\rangle/3\langle n_{\mathrm{st}}^{f\,2}\rangle^2)$, for different system sizes as shown in the inset in Fig. 2(a). Regarding the c electrons, we investigate the following observables: the Chern number C, computed with the method introduced in Ref. [56];

the density of states (DOS), $\mathrm{DOS}(\omega)=\sum_j\langle\delta(\omega-E_j(\{n_f\}))\rangle_{n_f}$; and the localization of the eigenstates, quantified by the inverse participation ratio (IPR) or detected by analyzing level spacing statistics (LSS). The IPR for the jth eigenstate is $\mathcal{I}_j=\sum_r|\langle r|\phi_j(\{n_f\})\rangle|^4$, where $\langle r|\phi_j(\{n_f\})\rangle$ is the amplitude of the eigenvector at site r, and we analyze the averaged quantity $\mathrm{IPR}(\omega)=\sum_j\langle\mathcal{I}_j\delta(\omega-E_j(\{n_f\}))\rangle_{n_f}/\mathrm{DOS}(\omega)$. The IPR scales to zero with the system's volume for extended states and to a constant for localized states. In the LSS analysis, level repulsion is expected for extended states, and the spacings between energy levels assume a Wigner distribution with standard deviation $\sigma/\langle s\rangle=0.422$ (for the unitary class to which the HFKM belongs), where $\langle s\rangle$ is the average value of the distribution of level spacings s; for localized states, the level spacing distribution acquires a Poisson-like shape with a larger $\sigma/\langle s\rangle$ [66]. In what follows, we describe the properties of the different phases in Fig. 1. A qualitatively similar phase diagram is also predicted with a mean-field approach [59].

CDW.—Below the T_{CDW} curve, the dashed-dotted (blue) line in Figs. 1 and 2(a), the f electrons start ordering in a checkerboard pattern for which only one of the sublattices is occupied as sketched in Fig. 2(a). To better understand the behavior of the CDW phase transition curve, we perform a mapping to the 2D antiferromagnetic Ising model at small and large U, and the phase transition curves can be obtained with a perturbative analysis [59]. These curves were computed up to second order in the perturbation and are shown in Fig. 2(a) as full (red) lines. For $U\ll 1$, $T_{\mathrm{CDW}}(U)\sim U^2$, whereas at large interactions, $T_{\mathrm{CDW}}(U)\sim U^{-1}$—the agreement with MC is remarkable.

Besides the expected trivial gapped CDW phase (MI-CDW), as found in Ref. [53] for the FKM, the HFKM additionally hosts a topological insulating phase with charge ordering (TI-CDW) along with a peculiar region of the phase diagram for which the c-electron spectrum is gapless inside the CDW phase (GI-CDW). The former had already been noticed in Refs. [33,67] and contrasts with the results of the Haldane model with NN interactions for which there is no region of coexistence between the CDW and TI phases [2]. Figure 2(b) shows the transition between gapped and gapless regimes in the MI-CDW and GI-CDW phases for $U=2.5$ and $L=16$. To ensure that the GI-CDW phase does not stem from a finite-size effect, we compute the DOS at the Fermi energy ($E=0$) in an energy window corresponding to 1% of the total bandwidth, decreasing its width proportionally to the system size. An example of this scaling is shown in Fig. 2(e) for a point inside the GI-CDW phase, for which it can be seen that the DOS ($E=0$) does not scale to zero.

TI and GTI.—The TI is a gapped topological phase, i.e., $\mathrm{DOS}(E)=0$ for $|E|<\Delta_{\mathrm{top}}/2$ and Chern number $C=1$, with Δ_{top} being the topological gap. At $T=0$, within the TI-CDW, the topological insulating phase exists between $U=0$ and $U=6\sqrt{3}t_2\approx 1$, the value at which the gap closes signaling the topological transition (TT) [54]. Upon increasing T, the topological phase extends to larger values of U. For $T\to\infty$, the system can be mapped to the Haldane model with quenched binary disorder, for which the disorder strength was reported to enhance the topological features [68]. In the present case, this translates to the extension of the topological phase to the $1\lessapprox U\lessapprox 2.7$ region for $T\gg 1$; see vertical lines in the phase diagram (Fig. 1). Our results show that temperature effects are responsible for an enhanced robustness of the topological state for all temperatures, which pushes the TT to larger values of U. The TT curve [69] is shown in Fig. 1 as a thin continuous (red) line [70]. The transition was determined by analyzing the finite-size scaling of the Chern number; see Fig. 3. Although the disorder effects are not of the same nature, a parallelism between the T-driven topological transition and the TAI phenomenon can be drawn. While in the latter quenched disorder is responsible for stabilizing topological phases, in the former thermal fluctuations play a similar role: They act as to promote an *annealed disorder* that can stabilize the topological phase.

We notice in Fig. 2(c) that the topological gap existing in the TI phase is closed in the GTI phase as one increases the interactions but the Chern number is unchanged ($C=1$), as can be seen in Fig. 3(b). For the TT from MI-CDW into the TI phase with increasing T, the gap closes and reopens at the transition curve. On the other hand, the TT from the GTI into the GI phase (analyzed below) is accompanied by the merging of the only two extended states that exist in the spectrum and carry opposite Chern numbers.

Topological phases are robust at finite T provided the thermal fluctuation energy k_BT does not exceed the energy separation of the extended states, as all the eigenstates in between are localized and cannot change the Chern number, similarly to the case of the integer quantum Hall effect. This condition breaks down near the TT curve in Fig. 1. However, as shown in Fig. 4(a), only slightly away from the TT line, the extended states already have an

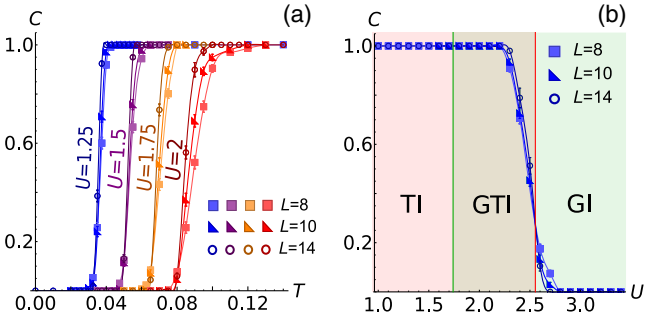

FIG. 3. Chern number computed through averages on Monte Carlo configurations of f electrons for different system sizes, with fixed U (a) and $T=0.2$ (b). The crossing points of these curves were used to obtain the topological transition curve in Fig. 1.

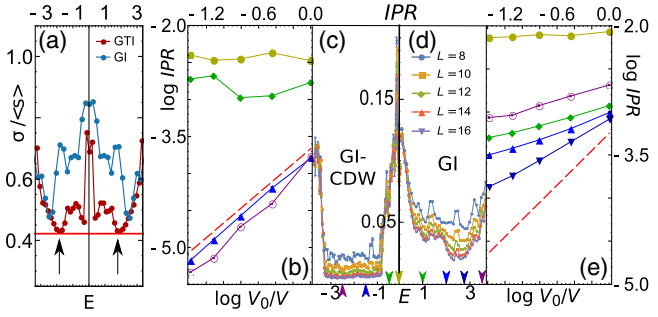

FIG. 4. (a) Standard deviations of the LSS distributions obtained for different energies in the GI [GTI] phase for $(U, T) = (2, 0.1)$ $[= (3.5, 0.2)]$ and $L = 14$. The horizontal (red) line corresponds to $\sigma/\langle s\rangle = 0.422$, which is the standard deviation of the Wigner distribution associated to extended states. The two extended states existing in the GTI phase are marked with arrows. (b) [(e)] Finite-size scaling of the IPR with the system volume V for the energies marked with the arrows in (c) [(d)], that shows the IPR for different sizes in the GI-CDW [GI] phase for $(U, T) = (2.5, 0.085)$ $[= (3.5, 0.2)]$. The IPR shown in (c) [(d)] for negative (positive) energies is symmetric in E. The red dashed lines shown in (b),(e) have a unit slope and indicate the scaling IPR $\sim V^{-1}$. The colors of the arrows that select specific energies in (c) [(d)] match the corresponding scaling curves in (b) [(e)].

energy separation $\Delta E \approx 4 \gg k_B T \approx 0.1$, allowing for a T-driven TT into gapped and gapless TIs.

GI and MI.—Increasing U from the GTI phase leads to an interaction-driven TT into a trivial gapless insulating phase (GI). If we continue increasing U, the c-electron spectrum acquires a Mott-like gap (MI). The corresponding DOS within the GI and MI phases is exemplified in Fig. 2(d). This transition resembles the one found for the 2D FKM in Ref. [53], for increasing interactions between an Anderson and a Mott insulator.

Gapless insulators.—We report, in Fig. 4(a), the LSS results for the GTI and GI phases. In the GTI phase, the standard deviation of the level spacing distributions, $\sigma/\langle s\rangle$, has the expected value for the Wigner distribution (horizontal line) at the particular energies corresponding to the two extended states that carry opposite Chern numbers. Away from these particular values, and within all the GI phase, $\sigma/\langle s\rangle$ raises above the Wigner distribution prediction signaling the localization of eigenstates. The IPR, for the GI phase, is depicted in Fig. 4(d). Around $E = 0$, it is almost unchanged with the system size; thus, the corresponding states are undoubtedly localized. However, for larger $|E|$ values, the IPR decreases with the system size. A finite-size analysis is shown in Fig. 4(e), where the unit slope associated with the scaling IPR $\propto V^{-1}$ is depicted by the (red) dashed line. Nonetheless, the slopes at different energies decrease with the system size, suggesting that localization is robust for every energy in the GI phase. These results are compatible with the following scenario: Outside the CDW phase, spatial correlations between f-electron occupations in GTI and GI phases decay exponentially with a characteristic length ξ. For distances larger than ξ, the disorder potential felt by the c electrons becomes uncorrelated. These phases smoothly extend to large T, for which $\xi \simeq 1$ and where disordered effects become equivalent to those of a binary quenched potential [68].

For the GI-CDW [Figs. 4(b) and 4(c)], a similar analysis suggests that, although the eigenstates are localized around $E = 0$, there are also regions of extended states. Figure 4(c) shows that the IPR becomes smaller with V for $-3 \lesssim E \lesssim -1$ (and $1 \lesssim E \lesssim 3$, not shown), and Fig. 4(b) indicates that, for two energies in this interval, the IPR indeed scales with V^{-1} for the used system sizes. This is in apparent contradiction with results for $\sigma/\langle s\rangle$ (not shown), where all energies rise above the Wigner distribution prediction indicating that all eigenstates should be localized. These seemingly contradicting facts can be reconciled by noticing that, inside the CDW phase, ξ diverges and the disordered potential experienced by the c electrons becomes long-range correlated. In two dimensions, systems with long-range spatially correlated disorder have been shown to support spectral regions of extended states [71–73]; moreover, Wigner distribution predictions are expected not to hold for such a kind of disorder.

Figure 1 shows that the GI-CDW phase is created, starting from the $T = 0$ gapped CDW, by increasing T. Our results show that the gap starts being populated by localized states induced by the thermal fluctuations. Here, again, disorder is correlated and may support extended states for a finite disorder strength. The important question is whether a region of extended states still survives upon entering the GI-CDW phase or if all states are already localized for this value of T. Although our results strongly suggest the former, we cannot definitely exclude the latter scenario, which will require working with substantially larger system sizes. If confirmed, the coexistence of spectral regions of extended and localized states would correspond to an interesting example of a many-body mobility edge in a strong interacting system and may suggest similar phenomena for a finite mass ratio between electronic species.

It is worth noting that the transverse conductance is quantized in the topological phases away from the crossover lines when the distance between the isolated extended states becomes larger than $k_B T$. This is because, in the gapless localized phases, since the model does not account for inelastic relaxation processes, the conductivity vanishes in the thermodynamic limit. For the gapped phases, the conductivity is exponentially suppressed $\sigma \sim \exp(-\Delta/k_B T)$ as long as the gap Δ is larger than $k_B T$.

Summarizing the central result of our work, we introduce the HFKM model, allowing one to effectively study the interplay of topology and interactions at finite temperatures and provide a complete characterization of the phase diagram. We observe a temperature-driven topological

transition into gapped and gapless topological insulators; finally, we find an insulating charge ordered state with gapless excitations where spectral regions of extended and localized states seem to coexist due to the long-range nature of the interaction-induced disorder potential.

All the ingredients for the experimental realization of the HFKM with ultracold atoms in optical lattices are separately available: There are recent implementations of mass unbalanced fermions [74,75], and the Haldane model has recently been successfully realized [76]. A direct verification of our results should therefore be achievable with state-of-the-art technology.

M. G., P. R., and E. V. C acknowledge partial support from FCT-Portugal through Grant No. UID/CTM/04540/2013. M. G. and P. R. acknowledge support by FCT-Portugal through the Investigador FCT Contract No. IF/00347/2014. R. M. acknowledges support of the NSFC Grants No. 11674021 and No. 11851110757 and NSAF-U1530401. The computations were performed in the Tianhe-2JK at the Beijing Computational Science Research Center (CSRC).

[1] C. Xu and J. E. Moore, Phys. Rev. B **73**, 045322 (2006).
[2] C. N. Varney, K. Sun, M. Rigol, and V. Galitski, Phys. Rev. B **82**, 115125 (2010).
[3] S. Rachel and K. Le Hur, Phys. Rev. B **82**, 075106 (2010).
[4] Y. Yamaji and M. Imada, Phys. Rev. B **83**, 205122 (2011).
[5] D. Zheng, G.-M. Zhang, and C. Wu, Phys. Rev. B **84**, 205121 (2011).
[6] S.-L. Yu, X. C. Xie, and J.-X. Li, Phys. Rev. Lett. **107**, 010401 (2011).
[7] C. Griset and C. Xu, Phys. Rev. B **85**, 045123 (2012).
[8] M. Hohenadler, T. C. Lang, and F. F. Assaad, Phys. Rev. Lett. **106**, 100403 (2011).
[9] M. Hohenadler, Z. Y. Meng, T. C. Lang, S. Wessel, A. Muramatsu, and F. F. Assaad, Phys. Rev. B **85**, 115132 (2012).
[10] J. Reuther, R. Thomale, and S. Rachel, Phys. Rev. B **86**, 155127 (2012).
[11] M. A. N. Araujo, E. V. Castro, and P. D. Sacramento, Phys. Rev. B **87**, 085109 (2013).
[12] M. Laubach, J. Reuther, R. Thomale, and S. Rachel, Phys. Rev. B **90**, 165136 (2014).
[13] R. S. K. Mong, A. M. Essin, and J. E. Moore, Phys. Rev. B **81**, 245209 (2010).
[14] C. Fang, M. J. Gilbert, and B. A. Bernevig, Phys. Rev. B **88**, 085406 (2013).
[15] T. Yoshida, R. Peters, S. Fujimoto, and N. Kawakami, Phys. Rev. B **87**, 085134 (2013).
[16] S. Miyakoshi and Y. Ohta, Phys. Rev. B **87**, 195133 (2013).
[17] S. Raghu, X.-L. Qi, C. Honerkamp, and S.-C. Zhang, Phys. Rev. Lett. **100**, 156401 (2008).
[18] J. Wen, A. Rüegg, C.-C. Joseph Wang, and G. A. Fiete, Phys. Rev. B **82**, 075125 (2010).
[19] J. C. Budich, R. Thomale, G. Li, M. Laubach, and S.-C. Zhang, Phys. Rev. B **86**, 201407 (2012).
[20] A. Dauphin, M. Müller, and M. A. Martin-Delgado, Phys. Rev. A **86**, 053618 (2012).
[21] C. Weeks and M. Franz, Phys. Rev. B **81**, 085105 (2010).
[22] L. Wang, X. Dai, and X. C. Xie, Europhys. Lett. **98**, 57001 (2012).
[23] A. Rüegg and G. A. Fiete, Phys. Rev. B **84**, 201103 (2011).
[24] K.-Y. Yang, W. Zhu, D. Xiao, S. Okamoto, Z. Wang, and Y. Ran, Phys. Rev. B **84**, 201104 (2011).
[25] N. A. García-Martínez, A. G. Grushin, T. Neupert, B. Valenzuela, and E. V. Castro, Phys. Rev. B **88**, 245123 (2013).
[26] M. Daghofer and M. Hohenadler, Phys. Rev. B **89**, 035103 (2014).
[27] J. Motruk, A. G. Grushin, F. de Juan, and F. Pollmann, Phys. Rev. B **92**, 085147 (2015).
[28] S. Capponi and A. M. Läuchli, Phys. Rev. B **92**, 085146 (2015).
[29] J. C. Budich, B. Trauzettel, and G. Sangiovanni, Phys. Rev. B **87**, 235104 (2013).
[30] S. Rachel, Rep. Prog. Phys. **81**, 116501 (2018), and references therein.
[31] Y.-X. Zhu, J. He, C.-L. Zang, Y. Liang, and S.-P. Kou, J. Phys. Condens. Matter **26**, 175601 (2014).
[32] Y.-H. Chen, H.-H. Hung, G. Su, G. A. Fiete, and C. S. Ting, Phys. Rev. B **91**, 045122 (2015).
[33] D. Zdulski and K. Byczuk, Phys. Rev. B **92**, 125102 (2015).
[34] Y.-Z. Chou, R. M. Nandkishore, and L. Radzihovsky, Phys. Rev. B **98**, 054205 (2018).
[35] T. Yoshida, S. Fujimoto, and N. Kawakami, Phys. Rev. B **85**, 125113 (2012).
[36] A. Rivas, O. Viyuela, and M. A. Martin-Delgado, Phys. Rev. B **88**, 155141 (2013).
[37] P. Dziawa, B. J. Kowalski, K. Dybko, R. Buczko, A. Szczerbakow, M. Szot, E. Lusakowska, T. Balasubramanian, B. M. Wojek, M. H. Berntsen, O. Tjernberg, and T. Story, Nat. Mater. **11**, 1023 (2012).
[38] A. Altland and M. R. Zirnbauer, Phys. Rev. B **55**, 1142 (1997).
[39] F. Evers and A. D. Mirlin, Rev. Mod. Phys. **80**, 1355 (2008).
[40] C.-K. K. Chiu, J. C. Y. Teo, A. P. Schnyder, and S. Ryu, Rev. Mod. Phys. **88**, 035005 (2016).
[41] M. Onoda and N. Nagaosa, Phys. Rev. Lett. **90**, 206601 (2003).
[42] M. Onoda, Y. Avishai, and N. Nagaosa, Phys. Rev. Lett. **98**, 076802 (2007).
[43] J. Li, R.-L. Chu, J. K. Jain, and S.-Q. Shen, Phys. Rev. Lett. **102**, 136806 (2009).
[44] C. W. Groth, M. Wimmer, A. R. Akhmerov, J. Tworzydło, and C. W. J. Beenakker, Phys. Rev. Lett. **103**, 196805 (2009).
[45] J. Song, H. Liu, H. Jiang, Q.-F. Sun, and X. C. Xie, Phys. Rev. B **85**, 195125 (2012).
[46] Y. Su, Y. Avishai, and X. R. Wang, Phys. Rev. B **93**, 214206 (2016).
[47] C. P. Orth, T. Sekera, C. Bruder, and T. L. Schmidt, Sci. Rep. **6**, 24007 (2016).
[48] L. M. Falicov and J. C. Kimball, Phys. Rev. Lett. **22**, 997 (1969).
[49] U. Brandt and R. Schmidt, Z. Phys. B **63**, 45 (1986).

[50] T. Kennedy and E. H. Lieb, Physica (Amsterdam) **138A**, 320 (1986).
[51] M. M. Maśka and K. Czajka, Phys. Rev. B **74**, 035109 (2006).
[52] M. Žonda, P. Farkašovský, and H. Čenčariková, Solid State Commun. **149**, 1997 (2009).
[53] A. E. Antipov, Y. Javanmard, P. Ribeiro, and S. Kirchner, Phys. Rev. Lett. **117**, 146601 (2016).
[54] F. D. M. Haldane, Phys. Rev. Lett. **61**, 2015 (1988).
[55] D. N. Sheng, L. Sheng, Z. Y. Weng, and F. D. M. Haldane, Phys. Rev. B **72**, 153307 (2005).
[56] Y.-F. Zhang, Y.-Y. Yang, Y. Ju, L. Sheng, R. Shen, D.-N. Sheng, and D.-Y. Xing, Chin. Phys. B **22**, 117312 (2013).
[57] E. V. Castro, M. P. López-Sancho, and M. A. H. Vozmediano, Phys. Rev. B **92**, 085410 (2015).
[58] E. V. Castro, R. de Gail, M. P. López-Sancho, and M. A. H. Vozmediano, Phys. Rev. B **93**, 245414 (2016).
[59] See Supplemental Material at http://link.aps.org/supplemental/10.1103/PhysRevLett.122.126601, which includes Refs. [60–65], for a brief description of the analysis on the perturbative results at large and small interactions and for the phase diagram of the HFKM obtained with the variational mean-field method.
[60] H. Ehrenreich, F. Seitz, and D. Turnbull, *Solid State Physics*, Solid State Physics Vol. 35 (Elsevier Science, New York, 1980).
[61] R. Haydock and C. M. M. Nex, J. Phys. C **17**, 4783 (1984).
[62] A. MacKinnon and B. Kramer, Phys. Rev. Lett. **47**, 1546 (1981).
[63] A. MacKinnon and B. Kramer, Z. Phys. B **53**, 1 (1983).
[64] K. Hoffmann and M. Schreiber, *Computational Physics: Selected Methods Simple Exercises Serious Applications* (Springer, Berlin, 2012).
[65] P. Coleman, *Introduction to Many-Body Physics* (Cambridge University Press, Cambridge, England, 2015).
[66] E. Prodan, J. Phys. A **44**, 113001 (2011).
[67] H.-S. Nguyen and M.-T. Tran, Phys. Rev. B **88**, 165132 (2013).
[68] M. Gonçalves, P. Ribeiro, and E. V. Castro, arXiv:1807.11247.
[69] Finite temperature transition lines correspond to sharp crossovers which occur within $k_B T$ around the drawn lines in Fig. 1 (up to intermediate temperatures), except for the CDW transition line which is well defined through the nullity of the associated order parameter.
[70] We notice that the small-U behavior of this curve has been qualitatively predicted with the mean field in Ref. [33].
[71] D. Taras-Semchuk and K. B. Efetov, Phys. Rev. B **64**, 115301 (2001).
[72] M. Hilke, Phys. Rev. Lett. **91**, 226403 (2003).
[73] F. A. De Moura, M. L. Lyra, F. Domínguez-Adame, and V. A. Malyshev, J. Phys. Condens. Matter **19**, 056204 (2007).
[74] G. Jotzu, M. Messer, F. Görg, D. Greif, R. Desbuquois, and T. Esslinger, Phys. Rev. Lett. **115**, 073002 (2015).
[75] D. Greif, G. Jotzu, M. Messer, R. Desbuquois, and T. Esslinger, Phys. Rev. Lett. **115**, 260401 (2015).
[76] G. Jotzu, M. Messer, R. Desbuquois, M. Lebrat, T. Uehlinger, D. Greif, and T. Esslinger, Nature (London) **515**, 237 (2014).